

Effect of fiber optic probe geometry on depth-resolved fluorescence measurements from epithelial tissues: a Monte Carlo simulation

Changfang Zhu, MEMBER SPIE
University of Wisconsin-Madison
Department of Electrical and Computer Engineering
Madison, Wisconsin 53706

Quan Liu, MEMBER SPIE
Nirmala Ramanujam, MEMBER SPIE
University of Wisconsin-Madison
Department of Biomedical Engineering
Madison, Wisconsin 53706
E-mail: nimmi@engr.wisc.edu

Abstract. Developing fiber optic probe geometries to selectively measure fluorescence spectra from different sublayers within human epithelial tissues will potentially improve the endogenous fluorescence contrast between neoplastic and nonneoplastic tissues. In this study, two basic fiber optic probe geometries, which are called the variable aperture (VA) and multidistance (MD) approaches, are compared for depth-resolved fluorescence measurements from human cervical epithelial tissues. The VA probe has completely overlapping illumination and collection areas with variable diameters, while the MD probe employs separate illumination and collection fibers with a fixed separation between them. Monte Carlo simulation results show that the total fluorescence detected is significantly higher for the VA probe geometry, while the probing depth is significantly greater for the MD probe geometry. An important observation is that the VA probe is more sensitive to the epithelial layer, while the MD probe is more sensitive to the stromal layer. The effect of other factors, including numerical aperture (NA) and tissue optical properties on the fluorescence measurements with VA and MD probe geometries, are also evaluated. The total fluorescence detected with both probe geometries significantly increases when the fiber NA is changed from 0.22 to 0.37. The sensitivity to different sublayers is found to be strongly dependent on the tissue optical properties. The simulation results are used to design a simple fiber optic probe that combines both the VA and MD geometries to enable fluorescence measurements from the different sublayers within human epithelial tissues. © 2003 Society of Photo-Optical Instrumentation Engineers. [DOI: 10.1117/1.1559058]

Keywords: probe geometry; fluorescence; Monte Carlo; epithelial tissue; precancer; neoplastic.

Paper JBO-02045 received Jul. 15, 2002; accepted for publication Oct. 29, 2002.

1 Introduction

Fluorescence spectroscopy has been widely explored for the detection of human epithelial precancers and early cancers.^{1–3} This technique has the capability to quickly, noninvasively, and quantitatively probe the biochemical and morphological changes in neoplastic tissues. In the last decade, a significant number of clinical investigations have demonstrated the diagnostic potential of fluorescence spectroscopy for differentiating neoplastic from nonneoplastic tissues in a variety of organ sites *in vivo*, including the colon, cervix, and bronchus.^{1–3}

A typical fluorescence spectroscopy system consists of a monochromatic excitation light source, an illumination and collection system, and a detector that can measure the emitted light as a function of wavelength. The geometry of the illumination and collection system is an important component of tissue fluorescence spectroscopy,⁴ and currently, fiber optic probes are predominantly used for this purpose.² Generally, fluorescence spectra are measured from epithelial tissues using fixed fiber optic probe geometries, i.e., the illumination and collection areas are fixed. A typical fiber optic probe has overlapping illumination and collection areas to minimize the effect of tissue turbidity,^{5,6} and the sampling area is usually 1

mm in diameter, such that fluorescence can be measured with sufficient signal-to-noise ratio. Interpreting the fluorescence measured with this probe geometry is usually complicated by the two-layered structure of epithelial tissue, which contains a superficial epithelium and an underlying stroma. The measured fluorescence may reflect the volume-averaged contributions from both sublayers.

Fluorescence contrast between neoplastic and nonneoplastic epithelial tissues is attributed to changes associated with several endogenous fluorophores, including tryptophan, reduced nicotinamide adenine dinucleotide (NADH), flavin adenine dinucleotide (FAD), and collagen.^{1,2} The distribution of these fluorophores is depth-dependent. The primary fluorophores in the epithelial layer are tryptophan, NADH, and FAD,^{7–10} while collagen is the dominant fluorophore in the stroma.⁸ Previous high resolution fluorescence imaging studies of unstained, frozen sections,^{11–22} fresh tissue slices,^{7,23,24} and freeze-trapped tissue blocks²⁵ indicate that the fluorescence intensity and distribution of the epithelial and stromal fluorophores alter with carcinogenesis. In particular, there is a

decrease in the collagen fluorescence within the stroma of neoplastic tissues relative to that of normal tissues. Within the epithelium, the NADH fluorescence of dysplastic regions is increased relative to that of normal epithelial cells, while the opposite result is observed for FAD. In addition, the thickness of the epithelium in tissues such as the cervix decreases with patient age⁷ and increases with dysplasia.^{23,24} Therefore it is important to be able to measure depth-resolved fluorescence from epithelial tissues in order to identify the origin of the fluorescence and to maximize the endogenous fluorescence contrast between neoplastic and nonneoplastic tissues.

Several studies have addressed the effect of illumination and collection geometries on probing fluorescence from different depths within tissue. Two basic probe geometries, the variable aperture (VA) and multidistance (MD) approaches have been evaluated. Pfefer et al.²⁶ used Monte Carlo simulations to investigate the effect of varying the diameter of a single optical fiber (which is used for both illumination and collection) on the fluorescence detected from a turbid medium. They showed that increasing the fiber diameter gives rise to an increase in the depth from which the detected fluorescent photons originate. With this information, Liu and Ramanujam²⁷ proposed a variable aperture probe for depth-dependent fluorescence measurements from a layered turbid medium simulating normal epithelial tissue and epithelial precancer. The variable aperture probe was designed to have completely overlapping illumination and collection areas and a range of aperture diameters. Monte Carlo simulations were carried out to assess the relationship between aperture diameter and the fluorescence detected from a fluorescent target (dysplastic region) embedded at different depths within a turbid medium (epithelial tissue). Their results showed that the variable aperture diameter at which maximum fluorescence is detected is directly related to the depth of the fluorescent target within the turbid medium. Hyde et al.²⁸ demonstrated the use of a multidistance probe to measure depth-resolved fluorescence from a layered turbid medium. The fiber optic probe they used consisted of 15 collection fibers located at increasing radial distances (1 to 10 mm) from a single illumination fiber, placed on the surface of a layered turbid medium. The spatially resolved fluorescence measured with this probe was used to describe the depth-dependent fluorophore concentra-

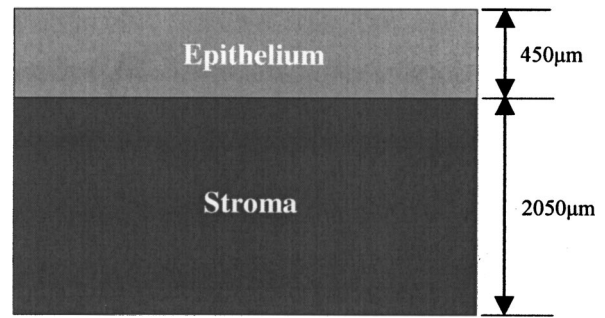


Fig. 1 The epithelial tissue model geometry, where the thickness of the epithelial layer and that of the stromal layer are fixed at 450 and 2050 μm, respectively.

tions of a fluorescent layer embedded at different depths within a homogeneous turbid medium.

We compared the VA and MD probe geometries for depth-resolved fluorescence measurements from epithelial tissues. In particular, Monte Carlo simulations were carried out to simulate fluorescence measurements from a two-layered epithelial tissue model of the human cervix using the VA and MD probe geometries. The quantitative endpoints evaluated are the total fluorescence detected, the probing depth, and the sensitivity to the epithelial and stromal layers of each probe geometry. The total fluorescence detected was significantly higher for the VA probe geometry, while the probing depth was significantly greater for the MD probe geometry. The VA probe was demonstrated to be more sensitive to the superficial epithelial layer, while the MD probe was observed to be more sensitive to the underlying stromal layer, for typical cervical epithelial tissue thicknesses.⁷ The total fluorescence detected with the VA and MD probe geometries was significantly increased with an increase in the fiber NA from 0.22 to 0.37. The sensitivity of the VA probe to the epithelial layer and that of the MD probe to the stromal layer were found to be strongly dependent on the tissue optical properties. The results of the simulations were used to design conceptually a simple fiber optic probe that combines both the VA and MD geometries to enable fluorescence measurements from the different sublayers within human epithelial tissues.

Table 1 Fluorescence efficiencies and optical properties (two optical property sets) designated for the epithelial and stromal layers in the epithelial tissue model. FE is the fluorescence efficiency, μ_a is the absorption coefficient, μ_s is the scattering coefficient, g is the anisotropy, n is the refractive index, λ_{exc} is the excitation wavelength, and λ_{emm} is the emission wavelength.

Optical property sets	Layers	FE at $\lambda_{exc} - \lambda_{emm}$ pair (460 to 520 nm)	μ_a, μ_s (1/cm), g and n at λ_{exc} (460 nm)	μ_a, μ_s (1/cm), g and n at λ_{emm} (520 nm)
Set 1	Epithelium	0.2	8.3, 110.3, 0.94, 1.37	5.3, 100.3, 0.94, 1.37
	stroma	0.6	8.3, 110.3, 0.94, 1.37	5.3, 100.3, 0.94, 1.37
Set 2	Epithelium	0.2	2.4, 94.0, 0.94, 1.37	1.8, 80.0, 0.94, 1.37
	stroma	0.6	5.0, 255.0, 0.94, 1.37	5.0, 220.0, 0.94, 1.37

2 Methods

2.1 Tissue Model Geometry and Optical Properties

A two-layer model was established to simulate human epithelial tissue, which consists of a superficial epithelium and an underlying stroma. Figure 1 depicts the epithelial tissue model geometry, where the thickness of the epithelial layer and that of the stromal layer are fixed at 450 and 2050 μm , respectively. A thickness of 450 μm was chosen for the epithelial layer to approximate the thickness of the human cervical epithelium.⁷ The thickness of the stromal layer was set at 2050 μm to represent an infinitely thick tissue. This thickness is far greater than the probing depth of the fiber optic probes employed in this study. This has been verified using Monte Carlo simulations. The lateral dimension of the model was assumed to infinite relative to the fiber optic probe dimensions used in this study (100 to 1000 μm).

Table 1 lists the fluorescence efficiencies and optical properties (two optical property sets) designated for the epithelial and stromal layers in the epithelial tissue model. The fluorescence was simulated at an excitation-emission wavelength pair of 460 to 520 nm. The primary endogenous fluorophore in epithelial tissue at this excitation-emission wavelength pair is flavin adenine dinucleotide (FAD).^{2,8} The fluorescence measured at this excitation-emission wavelength pair has been shown to be able to discriminate neoplastic from nonneoplastic human cervical tissues.^{25,29} For both optical property sets, the fluorescence efficiencies of the epithelial and stromal layers at 460 to 520 nm were defined from the results of previous human cervical tissue studies.²⁵ The two different optical property sets were employed in these simulations to allow for a general assessment of the different probe geometries. Optical properties and refractive indices for set 1 were obtained from the publication by Liu and Ramanujam.²⁷ In this set, optical properties were identical for both epithelial and stromal layers. Optical properties in set 2 were obtained from the publication by Drezek et al.²³ In this case, the epithelial layer and stromal layers have different absorption and scattering coefficients.

2.2 Illumination-Collection Geometries

Two illumination-collection geometries, the variable aperture (VA) and multidistance (MD) approaches, were employed to

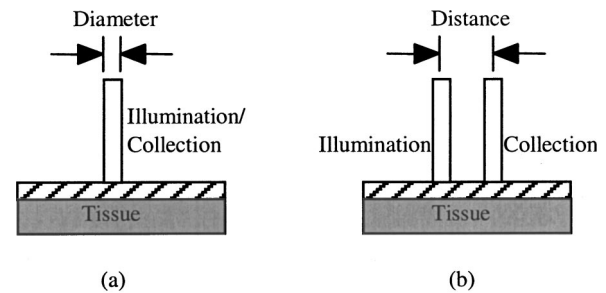


Fig. 2 Schematic of the (a) variable aperture (VA) and (b) multidistance (MD) probes. The VA probe has completely overlapping illumination and collection areas with variable diameters. In the MD approach, separate illumination and collection fibers are employed at a fixed separation on the tissue surface.

simulate fluorescence measurements from the epithelial tissue model. Figure 2 shows the schematic of the VA [Fig. 2(a)] and MD [Fig. 2(b)] probes. The VA probe has completely overlapping illumination and collection areas with variable diameters. In the MD approach, separate illumination and collection fibers are employed at a fixed separation on the tissue surface.

Table 2 provides the characteristics of the simulated VA and MD probe geometries. In VA, the illumination and collection diameters are equal to each other and are varied from 100 to 1000 μm in 100- μm increments. It should be noted that in this probe geometry, the illumination and collection areas completely overlap. Three MD probe geometries were studied: MD1, MD2, and MD3. In MD2, both the illumination and collection diameters are set at 200 μm . In MD1, the illumination diameter is increased to 900 μm , with no change to the collection diameter (compared to MD2). In MD3, the collection diameter is decreased to 100 μm , with no change to the illumination diameter (compared to MD2). In the MD probe geometry, there is one illumination fiber and there are five adjacent collection fibers, configured in a linear array. In the MD probe geometry, the center-to-center distance for each illumination-collection fiber pair is the distance between the center of the illumination fiber and the center of the particular collection fiber. Both fiber optic probe geometries were evaluated for numerical apertures (NAs) of 0.22 and 0.37.

Table 2 Characteristics of the simulated variable aperture (VA) and multidistance (MD) probe geometries. In the VA probe geometry, the illumination and collection areas completely overlap. In the MD probe geometry, the center-to-center distance for each illumination-collection fiber pair is the distance between the center of the illumination fiber and the center of the particular collection fiber.

Probe geometry	Illumination diameter (μm)	Collection diameter (μm)	Center-to-center distance (μm)	Numerical aperture
VA	100~1000	100~1000	0	0.22/0.37
MD1	900	200	550,750,950,1150,1350	0.22/0.37
MD2	200	200	200,400,600,800,1000	0.22/0.37
MD3	200	100	150,250,350,450,550	0.22/0.37

2.3 Monte Carlo Modeling

In this study, a modified, three-dimensional, weighted photon Monte Carlo code was employed to carry out fluorescence simulations on the theoretical model of human epithelial tissue using the VA and MD probe geometries. This code has been systematically validated by comparison of simulation results to experimental measurements on tissue phantom models for a range of optical properties representative of human epithelial tissues in the UV-visible spectrum and three different fiber optic probe geometries.³⁰ Two of the three fiber optic probe geometries are similar to MD1 and MD3. Details about the Monte Carlo simulation and its systematic validation are described in a companion manuscript, published in this issue.³⁰

2.4 Monte Carlo Simulation Parameters

In each Monte Carlo simulation, the excitation photons were launched at random, uniformly distributed locations over a range of angles defined by the NA and over a circular illumination area. To simulate fluorescence emission in the medium, a rejection scheme was used to determine whether or not the absorbed fraction of a photon packet is reemitted as a fluorescent photon. The fluorescent photons escaping the medium from the top surface were collected over a circular area defined by the collection diameter and over a range of exit angles within the NA. The circular illumination and collection areas are equivalent to the cross-sectional areas of the illumination and collection fibers, respectively. Since the illumination and collection fibers were assumed to be in direct contact with the tissue surface, the refractive index of the medium above the tissue model was set to be 1.452 to simulate an optical fiber, and that of the medium below the tissue model was set at 1.0. To simulate a 3-D tissue geometry in the computational model, a cylindrical coordinate system was used, in which the axial dimension is perpendicular to the top surface of the medium and the radial dimension corresponds to any direction perpendicular to the axial dimension. The axial and radial grid sizes were set at $10\ \mu\text{m}$, and the numbers of axial and radial grids were both set at 250 to define the volume of interest in the tissue model.

In this study, a total of ten million photons were launched to provide a balance between simulation accuracy and computational time. All the simulations were run on a 1.6-GHz Pentium 4 computer with a Windows 2000 operation system. The running time varied from a few hours to approximately a whole day. MATLAB 5.3 was used to perform postsimulation data processing and statistical analysis.

2.5 Analysis of the Simulation Results

The Monte Carlo simulation results were analyzed to enable comparison of the fluorescence measurements made with the VA and MD fiber optic probe geometries. A general summary of the comparison includes the following: total fluorescence detected, 80% probing depth, and sensitivity to the first (epithelial) layer. The total fluorescence detected was calculated by taking the ratio of the number of fluorescent photons detected by the collection fiber to the number of fluorescent photons generated within the epithelial tissue model. The 80% probing depth was defined as the depth within which 80% of the detected fluorescent photons originate. Here an 80% cri-

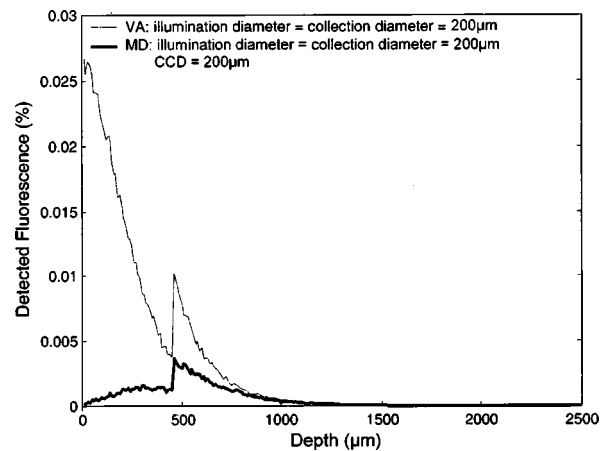


Fig. 3 The percent fluorescence detected with the VA and MD probes as a function of depth in the tissue. The depth-wise distribution was calculated by summing the number of fluorescent photons over all radial positions at a specific depth, and then dividing by the total number of fluorescent photons generated within the tissue model. Both the VA and MD probes have illumination and collection diameters of $200\ \mu\text{m}$ and an NA of 0.22. The separation between the illumination fiber and the collection fiber in the MD probe is $200\ \mu\text{m}$.

terion was used to evaluate the probing depth, within which the majority of the detected fluorescent photons originate. The sensitivity to the first layer was defined as the ratio of the detected fluorescence from the first layer (within the depth of $450\ \mu\text{m}$) to the total detected fluorescence.

3 Results

3.1 Depth-Resolved Fluorescence Profiles

Figure 3 shows the percent fluorescence detected with the VA and MD probes as a function of depth in the tissue. The depth-wise distribution was calculated by summing the number of fluorescent photons over all radial positions at a specific depth, and then dividing by the total number of fluorescent photons generated within the tissue model. Both the VA and MD probes have illumination and collection diameters of $200\ \mu\text{m}$, and an NA of 0.22. The separation between the illumination and collection fibers in the MD probe is $200\ \mu\text{m}$. Evaluation of Fig. 3 indicates that the fluorescence originating in the epithelial layer dominates the total fluorescence detected with the VA probe, while that originating in the stromal layer dominates the fluorescence detected with the MD probe. For both probe geometries, there is a significant increase in the detected fluorescence beyond a depth of $450\ \mu\text{m}$, which is due to the higher fluorescence efficiency of the stromal layer (0.6) versus the epithelial layer (0.2).

3.2 Variable Aperture Probe Geometry

Figures 4, 5, and 6 display the total fluorescence detected, the 80% probing depth, and the sensitivity to the first layer, respectively, for the variable aperture (VA) probe geometry. All the fibers have an NA of 0.22.

Figure 4 displays the total fluorescence detected from the epithelial tissue model with the VA probe. As the illumination/

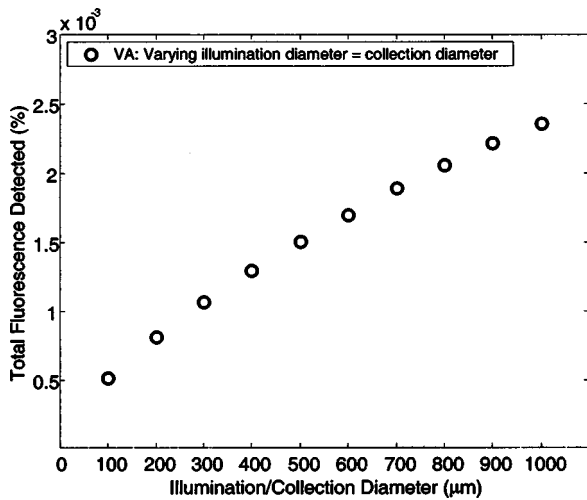


Fig. 4 The total fluorescence detected from the epithelial tissue model with the VA probe (see Table 2, NA=0.22). The total fluorescence detected was calculated by taking the ratio of the number of detected fluorescent photons to the number of fluorescent photons generated within the medium.

collection diameter increases from 100 to 1000 μm , the total fluorescence detected with VA probe increases from a minimum of $5\text{E-}4$ to a maximum of $2.5\text{E-}3$.

Figure 5 displays the 80% probing depth achieved in the epithelial tissue model with the VA probe. With the VA probe geometry, the 80% probing depth increases with the illumination/collection diameter from a minimum of ~ 300 μm to a maximum of ~ 750 μm .

Figure 6 displays the sensitivity to the first layer in the epithelial tissue model achieved with the VA probe. The sensitivity to the first layer of the VA probe decreases from a maximum of 90% to a minimum of 45% with an increase in the illumination/collection fiber diameter.

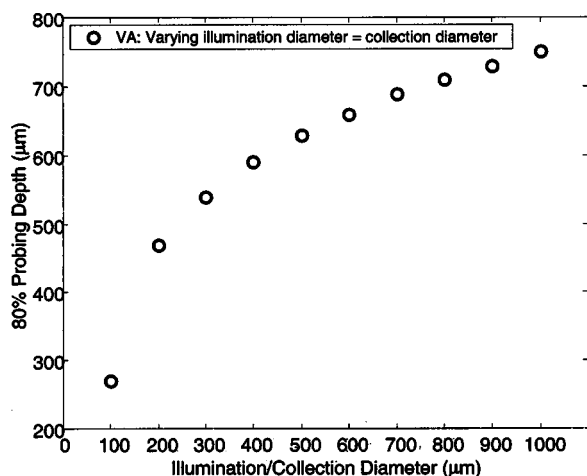


Fig. 5 The 80% probing depth achieved in the epithelial tissue model with the variable aperture (VA) probe (see Table 2, NA=0.22). The 80% probing depth is defined as the depth within which 80% of the detected fluorescent photons originate.

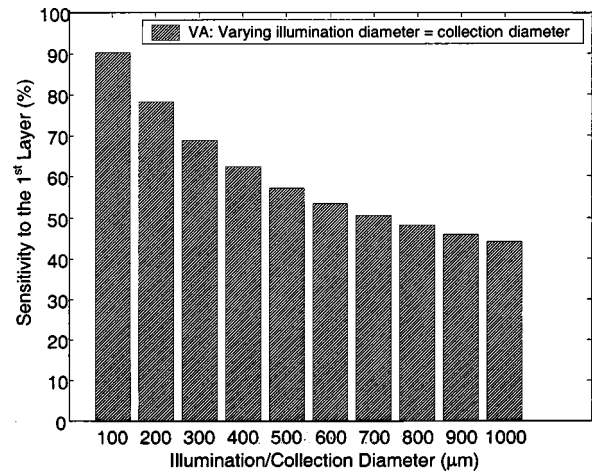


Fig. 6 The sensitivity to the first layer in the epithelial tissue model achieved with the variable aperture probe (see Table 2, NA=0.22). The sensitivity to the first layer is defined as the ratio of the detected fluorescence from the first layer (thickness of 450 μm) to the total detected fluorescence.

3.3 Multidistance Probe Geometry

Figures 7, 8, and 9 display the total fluorescence detected, the 80% probing depth and the sensitivity to the first layer, respectively, for three multidistance (MD) probe geometries: MD1, MD2, and MD3. In each of the MD probe geometries, the linearly arranged adjacent collection fibers are labeled 1 through 5, with number 1 corresponding to the nearest collection fiber and number 5 corresponding to the outermost one. The x axis indicates the collection fiber number, rather than the center-to-center distance between each collection fiber and the illumination fiber, as the latter is different for the three MD probe geometries. All the fibers have an NA of 0.22.

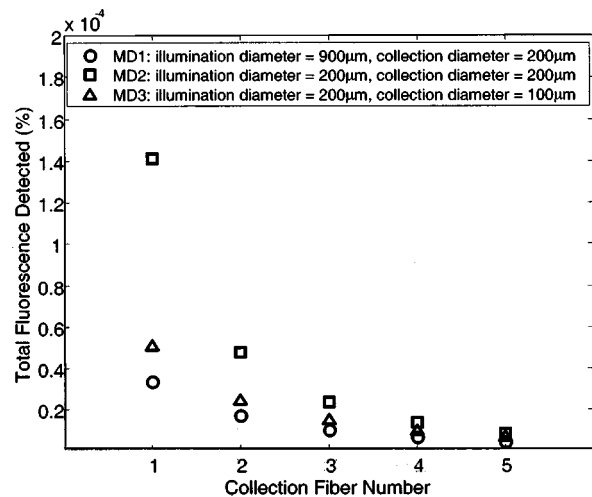


Fig. 7 The total fluorescence detected from the epithelial tissue model with the MD1, MD2, and MD3 probe geometries (see Table 2, NA = 0.22). The total fluorescence detected was calculated by taking the ratio of the number of detected fluorescent photons to the number of fluorescent photons generated within the medium. The linearly arranged adjacent collection fibers are labeled 1 through 5, with number 1 corresponding to the nearest collection fiber and number 5 corresponding to the outermost one.

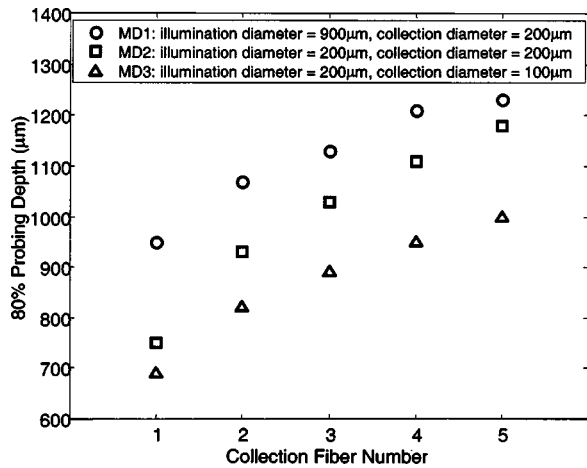


Fig. 8 The 80% probing depth in the epithelial tissue model achieved with the MD1, MD2, and MD3 probes (see Table 2, NA=0.22). The 80% probing depth is defined as the depth within which 80% of the detected fluorescent photons originate. The linearly arranged adjacent collection fibers are labeled 1 through 5, with number 1 corresponding to the nearest collection fiber and number 5 corresponding to the outermost one.

Figure 7 displays the total fluorescence detected from the epithelial tissue model with the MD1, MD2, and MD3 probe geometries. The total fluorescence detected ranges from a maximum of $1.5E-4$ to a minimum of $5E-6$ as the center-to-center distance between the illumination and collection fibers increases. At small center-to-center distances (for example, collection fiber 1), MD2 exhibits the highest total fluorescence detected among the three, followed by MD3, then MD1. At larger center-to-center distances (for example, collection fibers 4 and 5), the total fluorescence detected is very similar for the three probes. These results indicate that for a

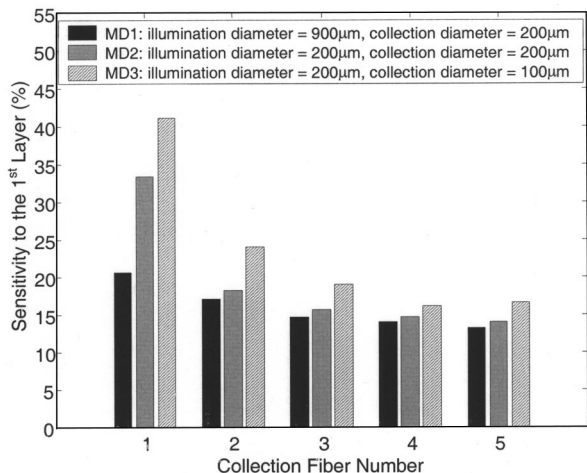


Fig. 9 The sensitivity to the first layer in the epithelial tissue model achieved with the MD1, MD2, and MD3 probes (see Table 2, NA = 0.22). The sensitivity to the first layer is defined as the ratio of the detected fluorescence from the first layer (thickness of $450 \mu\text{m}$) to the total detected fluorescence. The linearly arranged adjacent collection fibers are labeled 1 through 5, with number 1 corresponding to the nearest collection fiber and number 5 corresponding to the outermost one.

fixed collection diameter, less fluorescence is detected if the area over which the illumination photons are launched is increased (MD1 versus MD2). For a fixed illumination diameter, less fluorescence is detected if the collection area is decreased (MD3 versus MD2). The effect of varying the illumination and/or collection diameter diminishes as the center-to-center distance is increased.

Figure 8 shows the 80% probing depth in the epithelial tissue model achieved with the MD1, MD2, and MD3 probes. For the three probe geometries employed, the 80% probing depth increases from a minimum of $700 \mu\text{m}$ to a maximum of $1200 \mu\text{m}$, with an increase in the center-to-center distance between the illumination and collection fibers. MD1 has a greater probing depth than MD2, suggesting that an increase in the illumination diameter increases the probing depth. MD2 has a greater probing depth compared to MD3, indicating that increasing the collection diameter also increases the probing depth.

Figure 9 displays the sensitivity to the first layer in the epithelial tissue model achieved with the MD1, MD2, and MD3 probes. For all the three probe geometries, the sensitivity to the first layer ranges from a maximum of 40% to a minimum of 15%. At small center-to-center distances (for example, collection fiber 1), the sensitivity to the first layer is highest for MD3, followed by MD2, then MD1. At large center-to-center distances (for example collection fibers 4 and 5), the sensitivity to the first layer is very similar for all three probe geometries. These results suggest that increasing the illumination or collection diameter decreases the sensitivity to the first layer. The effect of varying the illumination and/or collection diameter diminishes as the center-to-center distance is increased.

3.4 Effect of Different Fiber Numerical Apertures

Table 3 shows the effect of two different fiber NAs (0.22 and 0.37) on the total fluorescence detected, the 80% probing depth, and the sensitivity to the first layer for the VA and MD2 probe geometries (see Table 2). The most significant change is observed in the total fluorescence detected, which is improved by a factor of 2 to 3 by increasing the NA from 0.22 to 0.37. The 80% probing depth is decreased only slightly when the NA is increased from 0.22 to 0.37. The sensitivity to the first layer does not change significantly as the fiber NA is increased from 0.22 to 0.37.

3.5 Effect of Optical Properties

Table 4 shows the effect of two different sets of optical properties (optical property sets 1 and 2, see Table 1) on the total fluorescence detected, the 80% probing depth, and the sensitivity to the first layer, for the VA and MD2 probe geometries (see Table 2) with an NA of 0.22. For convenience, the two sets of optical properties are denoted as tissue set 1 and tissue set 2, respectively. In tissue set 2, the absorption coefficient is lower in the first layer and the scattering coefficient is much higher in the second layer, relative to those in tissue set 1. The changes induced by different optical properties are different for the VA and MD2 probe geometries. In the case of the VA probe, the 80% probing depth is greater, while the total fluorescence detected and the sensitivity to the first layer is significantly lower for tissue set 2 compared to tissue set 1. In

Table 3 Effect of two different fiber numerical apertures (NAs) (0.22 and 0.37) on the total fluorescence detected, the 80% probing depth, and the sensitivity to the first layer for the VA and MD2 probe geometries (see Table 2). D_{ill} is the illumination diameter, D_{col} is the collection diameter, and CCD is the center-to-center distance between the illumination and the collection fiber.

		Total fluorescence detected (%)		80% Probing depth (μm)		Sensitivity to the first layer (%)	
		NA=0.22	NA=0.37	NA=0.22	NA=0.37	NA=0.22	NA=0.37
VA	$D_{\text{ill}}=D_{\text{col}}=100\ \mu\text{m}$	5.23E-04	1.25E-03	270	230	90.1916	91.4667
	$D_{\text{ill}}=D_{\text{col}}=300\ \mu\text{m}$	1.07E-03	2.82E-03	540	520	68.9646	71.4615
	$D_{\text{ill}}=D_{\text{col}}=500\ \mu\text{m}$	1.51E-03	4.10E-03	630	610	57.3006	59.7165
	$D_{\text{ill}}=D_{\text{col}}=700\ \mu\text{m}$	1.90E-03	5.16E-03	690	670	50.4026	51.7430
	$D_{\text{ill}}=D_{\text{col}}=900\ \mu\text{m}$	2.22E-03	6.17E-03	730	720	45.869	47.1951
MD2	CCD=200 μm	1.41E-04	3.95E-04	750	720	33.4278	36.0813
	CCD=400 μm	4.77E-05	1.38E-04	930	910	18.2962	17.0775
	CCD=600 μm	2.38E-05	7.01E-05	1030	1020	15.6343	14.5033
	CCD=800 μm	1.39E-05	4.14E-05	1110	1130	14.6207	14.9257
	CCD=1000 μm	8.80E-06	2.54E-05	1180	1150	13.9628	14.9556

the case of MD2, the 80% probing is slightly lower for tissue set 2 relative to tissue set 1, except at the shortest center-to-center distance. The total fluorescence detected is slightly higher for tissue set 2. The sensitivity to the first layer is significantly decreased for tissue set 2 compared to tissue set 1. In summary, the most significant finding is that for both VA and MD2 probe geometries, sensitivity to the first layer is

decreased when the absorption of the first layer is decreased and the scattering coefficient of the second layer is increased.

3.6 Comparison of VA and MD Probe Geometries

In summary, the VA and MD approaches have complementary characteristics. In Table 4, comparison of the VA and MD2

Table 4 The effect of two different sets of optical properties (optical property sets 1 and 2) on the total fluorescence detected, the 80% probing depth, and the sensitivity to the first layer for the variable aperture (VA) and multidistance (MD2) probe geometries (see Table 2) with a numerical aperture (NA) of 0.22. D_{ill} is the illumination diameter, D_{col} is the collection diameter, CCD is the center-to-center distance between the illumination and the collection fibers. For convenience, the two sets of optical properties are denoted as tissue set 1 and tissue set 2, respectively.

		Total fluorescence detected (%)		80% Probing depth (μm)		Sensitivity to the first layer (%)	
		Set 1	Set 2	Set 1	Set 2	Set 1	Set 2
VA	$D_{\text{ill}}=D_{\text{col}}=200\ \mu\text{m}$	8.15E-04	4.51E-04	470	600	78.2960	50.7892
	$D_{\text{ill}}=D_{\text{col}}=400\ \mu\text{m}$	1.30E-03	9.16E-04	590	700	62.3317	32.6273
	$D_{\text{ill}}=D_{\text{col}}=600\ \mu\text{m}$	1.70E-03	1.37E-03	660	750	53.4953	25.1728
	$D_{\text{ill}}=D_{\text{col}}=800\ \mu\text{m}$	2.06E-03	1.80E-03	710	790	47.9945	21.0432
	$D_{\text{ill}}=D_{\text{col}}=1000\ \mu\text{m}$	2.36E-03	2.20E-03	750	820	44.0251	18.7038
MD2	CCD=200 μm	1.41E-04	1.39E-04	750	780	33.4278	13.4367
	CCD=400 μm	4.77E-05	6.10E-05	930	910	18.2962	7.8590
	CCD=600 μm	2.38E-05	3.44E-05	1030	980	15.6343	7.0606
	CCD=800 μm	1.39E-05	2.18E-05	1110	1040	14.6207	7.3707
	CCD=1000 μm	8.80E-06	1.45E-05	1180	1080	13.9628	7.5215

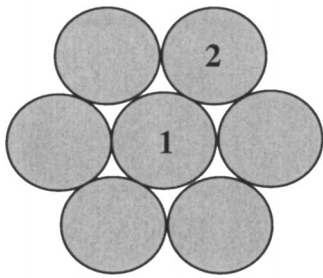


Fig. 10 Cross-section of a simple fiber optic probe design that combines the complementary characteristics of the VA and MD approach. The probe consists of seven optical fibers, each with a diameter of 200 μm . Three illumination and collection geometries can be implemented. First, the central fiber 1 can be used for both illumination and collection (VA approach: illumination diameter=collection diameter = 200 μm). Second, fiber 1 and fiber ring 2 can be used for illumination and collection (VA approach: illumination diameter=collection diameter=600 μm). Finally, fiber 1 can be used for illumination and fiber ring 2 can be used for collection (MD approach: illumination diameter=collection diameter=200 μm , center-to-center distance = 200 μm). All fibers have a numerical aperture (NA) of 0.22.

probe geometries indicates that for a fixed NA of 0.22 and for optical property set 1, the probing depth of the MD2 probe ranges from 750 to 1200 μm , while that of the VA probe ranges from 450 to 750 μm . At a similar probing depth of $\sim 750 \mu\text{m}$ for both the VA and MD2 probes, the total number of fluorescent photons detected by the VA probe is more than an order of magnitude greater than that detected by the MD2 probe. The sensitivity of the VA probe to the first layer ranges from 80 to 45%, while that of the MD2 probe ranges from 30 to 15%.

3.7 Combined VA and MD Probe Designs

The work shown here suggests that a fiber optic probe design that combines the VA and MD configurations can maximize the sensitivity to both the epithelial and stromal layer of epithelial tissues. Figure 10 shows the cross-section of a simple fiber optic probe design that combines the complementary characteristics of the VA and MD approach. The probe consists of seven optical fibers, each with a diameter of 200 μm . Three illumination and collection geometries can be implemented. First, the central fiber 1 can be used for both illumination and collection (VA approach: illumination diameter

= collection diameter=200 μm). Second, fiber 1 and fiber ring 2 can be used for illumination and collection (VA approach: illumination diameter=collection diameter = 600 μm). Finally, fiber 1 can be used for illumination and fiber ring 2 can be used for collection (MD approach: illumination diameter=collection diameter=200 μm , center-to-center distance=200 μm).

Table 5 shows the total fluorescence detected, the 80% probing depth, and the sensitivity to the first layer for the combined probe design shown in Fig. 10. The three different illumination and collection geometries allow the probing depth to vary such that at the smallest probing depth, the sensitivity to the first layer is maximized, while at the largest probing depth, the sensitivity to the second layer is maximized. At the intermediate probing depth, the probe samples both the first and second layer. The total fluorescence detected is lowest for the MD approach when one illumination and one collection fiber pair are simulated. In practice, this signal can be improved when a total of six collection fibers are used.

4 Discussion

We compared the VA and MD probe geometries for depth-resolved fluorescence measurements from epithelial tissues. The total fluorescence detected was significantly higher for the VA probe geometry, while the probing depth was significantly greater for the MD probe geometry. The VA probe was demonstrated to be more sensitive to the superficial epithelial layer, while the MD probe was observed to be more sensitive to the underlying stromal layer for typical cervical epithelial tissue thicknesses.⁷ The total fluorescence detected with the VA and MD probe geometries was significantly increased with an increase in the fiber NA from 0.22 to 0.37. The sensitivity of the VA probe to the epithelial layer and that of the MD probe to the stromal layer were found to be strongly dependent on the tissue optical properties. The results of the simulations were used to design a simple fiber optic probe that combines both the VA and MD geometries to enable fluorescence measurements from the different sublayers within human epithelial tissues.

The total number of fluorescent photons detected with the VA probe is much higher than that detected with the MD probe. In the VA geometry, the illumination and collection areas completely overlap, while in the MD geometry, the il-

Table 5 The total fluorescence detected, the 80% probing depth, and the sensitivity to the first layer for the combined probe design shown in Fig. 10. VA is the variable aperture probe geometry, MD is the multidistance probe geometry, D_{ill} is the illumination diameter, D_{col} is the collection diameter, and CCD is the center-to-center distance between the illumination and the collection fiber.

	VA ($D_{\text{ill}}=D_{\text{col}}=200 \mu\text{m}$)	VA ($D_{\text{ill}}=D_{\text{col}}=600 \mu\text{m}$)	MD ($D_{\text{ill}}=D_{\text{col}}=200 \mu\text{m};$ CCD=200 μm)
Total fluorescence detected (%)	8.15E-04	1.70E-03	1.41E-04 × six collection fibers
80% Probing depth (μm)	470	660	750
Sensitivity to the epithelial layer (%)	78	54	33

illumination and collection areas are completely separated. In a direct tissue-fiber contact mode, an increase in the overlap between the illumination and collection areas will increase the total fluorescence detected. In the VA approach, the total fluorescence detected increases with increasing illumination/collection diameter, as would be expected. Similarly, in the MD approach, the total fluorescence detected increases with the collection diameter. However, an increase in the illumination diameter results in a decrease in the total detected fluorescence for the MD probe. The findings related to the illumination diameter are counterintuitive. However, they can be explained by the fact that when the illumination diameter is increased, so that excitation photons are launched over a greater area, the number of excitation photons per unit area is decreased. This results in a decrease in the number of emitted fluorescent photons per unit area. In the case of MD probe geometry, the greater the separation between illumination and collection fiber, the less fluorescence is detected. The primary reason for this trend is that a large portion of fluorescence generated in the medium originates within the region directly below the illumination fiber. Thus the lateral distribution of emitted fluorescence decreases with increasing distance from this region.

The VA probe has a smaller probing depth and is highly sensitive to the epithelial layer, while the MD probe has a greater probing depth and is more sensitive to the stromal layer. Furthermore, increasing the illumination/collection diameter in either the VA or MD approach increases probing depth and decreases the sensitivity to the first layer. The basis for this observation is that the deeper the fluorescent photon is emitted within the medium, the greater the chance that it will travel a longer lateral distance before escaping the medium. In other words, fluorescence originating deeper in the medium is more likely to be detected at a distant location from the illuminated area.

Variations in NA from 0.22 to 0.37 only have a slight impact on sublayer sensitivity and probing depth. However, increasing the NA results in a significant improvement in the total fluorescence detected. This effect is due to a larger acceptance angle, which gives rise to an increase in the overlap between the illumination and collection areas.

Variation in the optical properties does not, for the most part, alter the basic differences between the VA and MD probe geometries. For both sets of tissue optical properties, the VA geometry has a lower probing depth, higher total fluorescence detected, and higher sensitivity to the first layer, compared to the MD geometry. Within the VA approach, a change in the optical properties from set 1 to set 2 decreases the total fluorescence detected and the sensitivity to the first layer, and increases the probing depth. Within the MD approach, changing the optical properties from set 1 to set 2 slightly increases the total fluorescence detected, while decreasing the sensitivity to the first layer and the probing depth. These observed trends may be attributed to the differences in the absorption and scattering coefficients of the epithelial and stromal layer, which alter fluorescent light transport inside the medium. In tissue set 2, the absorption coefficient is lower in the first layer and the scattering coefficient is much higher in the second layer, relative to that in tissue set 1. The predominant effect of these changes is that less excitation photons are absorbed in the first layer, so that the number of excitation pho-

tons that reach the second layer increases. This results in less fluorescence originating in the first layer and more fluorescence originating in the second layer. This implies a decrease in the sensitivity to the first layer for both the VA and MD probes. Since the VA probe is more sensitive to the first layer, the decrease in fluorescence originating in the first layer results in a decrease in the total fluorescence detected with the VA probe. At the same time, the number of detected fluorescent photons that originate in the second layer increases, so that the VA probe achieves a greater probing depth into the second layer. On the contrary, since the MD probe is more sensitive to the second layer, an increase in fluorescence originating in the second layer results in an increase in the total fluorescence detected with the MD probe. Furthermore, most of the fluorescence detected with the MD probe originates within the upper region of the second layer, where the most significant increase in the originating fluorescence is observed. Therefore the thickness of the tissue region from which the vast majority of detected fluorescence originates is decreased, i.e. the probing depth that the MD probe achieves is decreased.

The primary objective of this study is to quantify the basic characteristics of two fiber optic probe geometries, VA and MD, for depth-resolved fluorescence measurements from epithelial tissue. A secondary objective was to evaluate whether varying the optical properties would alter the general characteristics of the two probe geometries. Thus, only two sets of specific optical properties were assessed. The results indicate that the probing depth, total detected fluorescence, and sensitivity to different sublayers of the two probe geometries are subject to change with different optical properties; however, the basic characteristics of the two probe geometries are not altered. A more quantitative assessment of the effect of a wide range of optical properties on the VA and MD probe geometries is beyond the scope of the current study, but will be interesting to explore in future investigations.

The work addressed here indicates that VA and MD approaches have complementary characteristics. It would be appropriate to combine both geometries to achieve maximum sensitivity to both the epithelial and stromal layers. Figure 10 gives an example of such a probe design. The total fluorescence detected is of much concern in practice. The data listed in Table 5 shows that the total fluorescence detected is lowest for the MD probe geometry that employs a single illumination and collection fiber pair. The MD configuration shown here has been used to measure fluorescence from the hamster cheek pouch.³¹ Specifically, a fiber optic probe with a single illumination and a single collection fiber, each with a diameter of 214 μm and a 0.22 numerical aperture, were employed. The two fibers were adjacently placed at a center-to-center distance of approximately 245 μm . Hamster oral epithelial tissue fluorescence spectra were measured with a signal-to-noise ratio of greater than 35:1 at the fluorescence maxima at a wide range of excitation wavelengths over the entire UV-visible region. Thus, it is feasible to measure the depth resolved fluorescence of epithelial tissues using the proposed probe design. It should be noted that the probe design shown in Fig. 10, is just one example of a number of possible probe configurations. The probe geometry for a specific clinical application will depend on the fluorescence efficiencies, optical properties, tissue geometry, and depth of interest in the tissue.

In practice, it is relatively straightforward to implement the MD probe geometry. The illumination fiber(s) can be coupled to the light source and the collection fiber(s) can be coupled to the detector. It is more complex to implement the VA probe geometry, since additional optical components (lenses and beamsplitter) are needed to couple one fiber (that serves to illuminate and collect) to both the light source and the detector. An alternative way to achieve the VA probe geometry is to have the overlapping illumination and collection aperture be made up of several optical fibers, each with a cross-sectional diameter, that is smaller than that of the VA cross-sectional diameter (for example, a VA probe with a cross-sectional diameter of 600 μm can be made up of seven optical fibers, each with a cross-sectional diameter of 200 μm). Approximately 50% of the optical fibers can be used for illumination (i.e., coupled to the light source), and the remaining 50% can be used for collection (i.e., coupled to the detector). The limitation of this approach is that it will be practically difficult in designing VA probes with multiple individual optical fibers for VA probes with small cross-sectional diameters (such as 100 μm).

In conclusion, this study demonstrates that the total fluorescence detected, the probing depth, and the sensitivity to the epithelial/stromal layer in epithelial tissues are highly dependent on the fiber optic probe geometry used (VA versus MD probe geometry). These simulations suggest that by combining complementary illumination-collection geometries, a simple probe can be developed for depth-resolved fluorescence measurements from epithelial tissues.

Acknowledgments

The authors would like to acknowledge the assistance of Erin Gill and Chris Khoury for their involvement in the generation of preliminary ideas for this project. The authors would also like to acknowledge NIH (PO1 CA82710-01) for supporting this work.

References

1. R. Richards-Kortum and E. Sevick-Muraca, "Quantitative optical spectroscopy for tissue diagnosis," *Annu. Rev. Phys. Chem.* **47**, 555–606 (1996).
2. N. Ramanujam, "Fluorescence spectroscopy of neoplastic and non-neoplastic tissues," *Neoplasia* **2**, 89–117 (2000).
3. G. A. Wagnieres, W. M. Star, and B. C. Wilson, "In vivo fluorescence spectroscopy and imaging for oncological applications," *Photochem. Photobiol.* **68**, 603–632 (1998).
4. M. Keijzer, R. R. Richards Kortum, S. L. Jacques, and M. S. Feld, "Fluorescence spectroscopy of turbid media: autofluorescence of the human aorta," *Appl. Opt.* **28**, 4286–4292 (1989).
5. J. Qu, C. MacAulay, S. Lam, and B. Palcic, "Laser-induced fluorescence spectroscopy at endoscopy: tissue optics, Monte Carlo modeling, and in vivo measurements," *Opt. Eng.* **34**(11), 3334–3343 (1995).
6. R. Richards-Kortum, A. Mehta, G. Hayes, R. Cothren, T. Kolubayev, C. Kittrell, N. B. Ratliff, J. R. Kramer, and M. S. Feld, "Spectral diagnosis of atherosclerosis using an optical fiber laser catheter," *Am. Heart J.* **118**, 381–391 (1989).
7. C. K. Brookner, M. Follen, I. Boiko, J. Galvan, S. Thomsen, A. Malpica, S. Suzuki, R. Lotan, and R. Richards-Kortum, "Autofluorescence patterns in short-term cultures of normal cervical tissue," *Photochem. Photobiol.* **71**, 730–736 (2000).
8. K. Sokolov, J. Galvan, A. Myakov, A. Lacy, R. Lotan, and R. Richards-Kortum, "Realistic three-dimensional epithelial tissue phantoms for biomedical optics," *J. Biomed. Opt.* **7**, 148–156 (2002).
9. J. D. Pitts, R. D. Sloboda, K. H. Dragnev, E. Dmitrovsky, and M. A. Mycek, "Autofluorescence characteristics of immortalized and carcinogen-transformed human bronchial epithelial cells," *J. Biomed. Opt.* **6**, 31–40 (2001).
10. D. L. Heintzelman, R. Lotan, and R. R. Richards-Kortum, "Characterization of the autofluorescence of polymorphonuclear leukocytes, mononuclear leukocytes and cervical epithelial cancer cells for improved spectroscopic discrimination of inflammation from dysplasia," *Photochem. Photobiol.* **71**, 327–332 (2000).
11. W. Lohmann and E. Paul, "Native fluorescence of unstained cryosections of the skin with melanomas and nevi," *Naturwissenschaften* **76**, 424–426 (1989).
12. K. Izuishi, H. Tajiri, T. Fujii, N. Boku, A. Ohtsu, T. Ohnishi, M. Ryu, T. Kinoshita, and S. Yoshida, "The histological basis of detection of adenoma and cancer in the colon by autofluorescence endoscopic imaging," *Endoscopy* **31**, 511–516 (1999).
13. H. W. Wang, J. Willis, M. I. Canto, M. V. Sivak, and J. A. Izatt, "Quantitative laser scanning confocal autofluorescence microscopy of normal, premalignant, and malignant colonic tissues," *IEEE Trans. Biomed. Eng.* **46**, 1246–1252 (1999).
14. G. Bottioli, A. C. Croce, D. Locatelli, R. Nano, E. Giombelli, A. Messina, and E. Benericetti, "Brain tissue autofluorescence: an aid for intraoperative delineation of tumor resection margins," *Cancer Detect. Prev.* **22**, 330–339 (1998).
15. A. Fryen, H. Glanz, W. Lohmann, T. Dreyer, and R. M. Bohle, "Significance of autofluorescence for the optical demarcation of field cancerisation in the upper aerodigestive tract," *Acta Oto-Laryngol.* **117**, 316–319 (1997).
16. G. Bottioli, A. C. Croce, D. Locatelli, R. Marchesini, E. Pignoli, S. Tomatis, C. Cuzzoni, S. Di Palma, M. Dalfante, and P. Spinelli, "Natural fluorescence of normal and neoplastic human colon: a comprehensive ex vivo study," *Lasers Surg. Med.* **16**, 48–60 (1995).
17. G. S. Fiarman, M. H. Nathanson, A. B. West, L. I. Deckelbaum, L. Kelly, and C. R. Kapadia, "Differences in laser-induced autofluorescence between adenomatous and hyperplastic polyps and normal colonic mucosa by confocal microscopy," *Dig. Dis. Sci.* **40**, 1261–1268 (1995).
18. T. J. Romer, M. Fitzmaurice, R. M. Cothren, R. Richards-Kortum, R. Petras, M. V. Sivak, and J. R. Kramer, "Laser-induced fluorescence microscopy of normal colon and dysplasia in colonic adenomas: implications for spectroscopic diagnosis," *Am. J. Gastroenterol.* **90**, 81–87 (1995).
19. G. I. Zonios, R. M. Cothren, J. T. Arendt, J. Wu, J. Van Dam, J. M. Crawford, R. Manoharan, and M. S. Feld, "Morphological model of human colon tissue fluorescence," *IEEE Trans. Biomed. Eng.* **43**, 113–122 (1996).
20. W. Lohmann, B. Hirzinger, J. Braun, K. Schwemmler, K. H. Muhrer, and A. Schulz, "Fluorescence studies on lung tumors," *Z. Naturforsch. [C]* **45**, 1063–1066 (1990).
21. W. Lohmann and S. Kunzel, "Fluorescence tomographical studies on breast tissue with cancer," *Naturwissenschaften* **77**, 476–478 (1990).
22. W. Lohmann, J. Mussmann, C. Lohmann, and W. Kunzel, "Native fluorescence of unstained cryo-sections of the cervix uteri compared with histological observations," *Naturwissenschaften* **76**, 125–127 (1989).
23. R. Drezek, K. Sokolov, U. Utzinger, I. Boiko, A. Malpica, M. Follen, and R. Richards-Kortum, "Understanding the contributions of NADH and collagen to cervical tissue fluorescence spectra: modeling, measurements, and implications," *J. Biomed. Opt.* **6**, 385–396 (2001).
24. R. Drezek, C. Brookner, I. Pavlova, I. Boiko, A. Malpica, R. Lotan, M. Follen, and R. Richards-Kortum, "Autofluorescence microscopy of fresh cervical-tissue sections reveals alterations in tissue biochemistry with dysplasia," *Photochem. Photobiol.* **73**, 636–641 (2001).
25. N. Ramanujam, R. Richards Kortum, S. Thomsen, A. Mahadevan Jansen, M. Follen, and B. Chance, "Low temperature fluorescence imaging of freeze-trapped human cervical tissues," *Opt. Express* **8**, 335–343 (2001).
26. T. J. Pfefer, K. T. Schomacker, M. N. Ediger, and N. S. Nishioka, "Light propagation in tissue during fluorescence spectroscopy with single-fiber probes," *IEEE J. Sel. Top. Quantum Electron.* **7**, 1004–1012 (2001).
27. Q. Liu and N. Ramanujam, "Relationship between depth of a target in a turbid medium and fluorescence measured by a variable-aperture method," *Opt. Lett.* **27**, 104–106 (2002).
28. D. E. Hyde, T. J. Farrell, M. S. Patterson, and B. C. Wilson, "A diffusion theory model of spatially resolved fluorescence from depth-

- dependent fluorophore concentrations," *Phys. Med. Biol.* **46**, 369–383 (2001).
29. U. Utzinger, E. V. Trujillo, E. N. Atkinson, M. F. Mitchell, S. B. Cantor, and R. Richards-Kortum, "Performance estimation of diagnostic tests for cervical precancer based on fluorescence spectroscopy: effects of tissue type, sample size, population, and signal-to-noise ratio," *IEEE Trans. Biomed. Eng.* **46**, 1293–1303 (1999).
 30. Q. Liu, C. Zhu, and N. Ramanujam, "Experimental validation of Monte Carlo modeling of fluorescent light propagation in the UV-visible spectrum," *J. Biomed. Opt.* **8**, 223–236 (2003).
 31. G. M. Palmer, C. L. Marshak, K. M. Vrotsos, and N. Ramanujam, "Optimal methods for fluorescence and diffuse reflectance measurements of tissue biopsy samples," *Lasers Surg. Med.* **30**, 191–200 (2002).